

# ATLAS discovery potential for a heavy charged Higgs boson

Kétévi Adiklè Assamagan

Department of Physics, Brookhaven National Laboratory  
Upton, NY 11973 USA

Yann Coadou

Department of Radiation Sciences, Uppsala University  
Box 535, 751 21 Uppsala, Sweden

Aldo Deandrea

Institut de Physique Nucléaire, Université de Lyon I  
4 rue E. Fermi, F-69622 Villeurbanne Cedex, France

## Abstract

The sensitivity of the ATLAS detector to the discovery of a heavy charged Higgs boson is presented. Assuming a heavy SUSY spectrum, the most promising channels above the top quark mass are  $H^\pm \rightarrow tb$  and  $H^\pm \rightarrow \tau^\pm \nu_\tau$  which provide coverage in the low and high  $\tan \beta$  regions up to  $\sim 600$  GeV. The achievable precisions on the charged Higgs mass and  $\tan \beta$  determination are also discussed. The  $H^\pm \rightarrow W^\pm h^0$  channel, though restricted to a small MSSM parameter space, shows a viable signal in NMSSM where the parameter space is less constrained. The observation of the channel  $H^- \rightarrow \tau_L^- \nu_\tau + c.c.$  may constitute a distinctive evidence for models with singlet neutrinos in large extra dimensions.

PACS: 14.80.Cp, 12.60.Jv, 11.10.Kk

LYCEN-2002-10  
BNL-68986  
ATL-COM-PHYS-2002-002  
SN-ATLAS-2002-017  
February 2002

# ATLAS discovery potential for a heavy charged Higgs boson

K  t  vi A. Assamagan\*

*Department of Physics, Brookhaven National Laboratory, Upton, NY 11973 USA*

Yann Coadou†

*Department of Radiation Sciences, Uppsala University, Box 535, 751 21 Uppsala, Sweden*

Aldo Deandrea‡

*Institut de Physique Nucl  aire, Universit   Lyon I,  
4 rue E. Fermi, F-69622 Villeurbanne Cedex, France*

(Dated: February, 2002)

The sensitivity of the ATLAS detector to the discovery of a heavy charged Higgs boson is presented. Assuming a heavy SUSY spectrum, the most promising channels above the top quark mass are  $H^\pm \rightarrow tb$  and  $H^\pm \rightarrow \tau^\pm \nu_\tau$  which provide coverage in the low and high  $\tan \beta$  regions up to  $\sim 600$  GeV. The achievable precisions on the charged Higgs mass and  $\tan \beta$  determination are also discussed. The  $H^\pm \rightarrow W^\pm h^0$  channel, though restricted to a small MSSM parameter space, shows a viable signal in NMSSM where the parameter space is less constrained. The observation of the channel  $H^- \rightarrow \tau_L^- \nu_\tau + c.c.$  may constitute a distinctive evidence for models with singlet neutrinos in large extra dimensions.

PACS numbers: 14.80.C, 12.60.Jv, 11.10.Kk

## I. INTRODUCTION

In the Standard Model (SM), one scalar doublet is responsible for the electroweak symmetry breaking, leading to the prediction of one neutral scalar particle in the physical spectrum, the Higgs boson. The spectrum of many extensions to the SM includes a charged Higgs state. We consider as a prototype of these models the two-Higgs Doublet Model of type II (2HDM-II), where the Higgs doublet with hypercharge  $-1/2$  couples only to right-handed up-type quarks and neutrinos whereas the  $+1/2$  doublet couples only to right-handed charged leptons and down-type quarks; an example is the Minimal Supersymmetric Standard Model (MSSM). In the following we will use the vacuum expectation values (VEV)  $v \simeq 246$  GeV of the SM and  $v_1$  (VEV of the  $+1/2$  doublet) and  $v_2$  (VEV of the  $-1/2$  doublet) of the 2HDM. They relate to each other as:

$$\frac{v}{\sqrt{2}} = \sqrt{v_1^2 + v_2^2} \quad \tan \beta = \frac{v_2}{v_1} \quad (1)$$

and the tree level relation to the  $W$  mass is  $m_W^2 = g^2 v^2 / 4 = g^2 (v_1^2 + v_2^2) / 2$ . In the 2HDM models, the two complex Higgs doublets correspond to eight scalar states. Symmetry breaking leads to five Higgs bosons, three neutral (two CP-even  $h$ ,  $H$  and one CP-odd  $A$ ) and a charged pair,  $H^\pm$  [1]. At tree level, the Higgs sector of the MSSM is specified by two parameters, generally taken as  $m_A$ , the mass of the CP-odd Higgs  $A$  and  $\tan \beta$ , the ratio of

the vacuum expectation values of the two Higgs doublets. However, radiative corrections can modify tree level relations significantly — the most affected is the mass of the lightest CP-even Higgs which is constrained at tree level to be below  $m_Z$  but with radiative corrections, the upper bound is shifted to  $\sim 135$  GeV [2]. While the neutral Higgs bosons may be difficult to distinguish from the one of the SM, the charged Higgs bosons are a distinctive signal of physics beyond the SM. The detection of a  $H^\pm$  may therefore play an important role in the discovery of an extended Higgs sector, such as the one required by the MSSM.

LEP searches have yielded a lower bound of 114.1 GeV on the mass of the SM Higgs boson with a  $2.1\sigma$  evidence for a 115.6 GeV Higgs [3]. An upper bound of 196 GeV on the SM Higgs boson mass is inferred from global fits to precision electroweak data [4]. At the Tevatron Run 1, the SM Higgs boson has been searched for in the process  $q\bar{q} \rightarrow Z(W)H$  where the associated vector boson provides a suppression of the backgrounds. These searches yield no evidence of the Higgs as the observed events are consistent with expectation from the backgrounds [5]. The search for the SM Higgs boson will be continued at the Tevatron where the mass range covered will be extended to  $\sim 170$  GeV with an integrated luminosity of up to  $\sim 40$   $\text{fb}^{-1}$ . At the LHC (Large Hadron Collider), a SM Higgs signal can be observed with a significance of more than  $5\sigma$  after just several months of data taking ( $< 10$   $\text{fb}^{-1}$ ).

In the MSSM, lower bounds of 91.0 and 91.9 GeV on the masses of the lightest CP-even Higgs  $h$  and the CP-odd Higgs  $A$  have been set in the experimental searches at LEP. Further, the  $\tan \beta$  regions of  $0.5 < \tan \beta < 2.4$  and  $0.7 < \tan \beta < 10.5$  are excluded at 95% confidence level for the maximum  $m_h$  and the no-mixing scenarios

---

\*Electronic address: ketevi@bnl.gov

†Electronic address: yann@tsl.uu.se

‡Electronic address: deandrea@ipnl.in2p3.fr

respectively [3]. In addition, a large area of the 2HDM-II parameter space has been scanned leading to the exclusion at 95% CL of significant regions of the  $(m_h, m_A)$ ,  $(m_h, \tan \beta)$  and  $(m_A, \tan \beta)$  projections. Within the scanned parameter space, the region  $1 \lesssim m_h \lesssim 44$  GeV and  $12 \lesssim m_A \lesssim 56$  GeV is excluded at 95% CL independent of  $\tan \beta$  and  $\alpha$  [6]. A model-independent interpretation, with no assumption made on the structure of the Higgs sector, was also conducted at LEP. Lower bounds are set at 95% CL on the masses of the scalar and pseudo-scalar neutral Higgs bosons  $S^0$  and  $P^0$  — in the search for the generic processes  $e^+e^- \rightarrow S^0Z^0$  and  $e^+e^- \rightarrow S^0P^0$  — depending on the assumed values of the scale factors  $s^2$  and  $c^2$ , and of the branching ratios [6]. At the Tevatron, the lightest Higgs boson of MSSM has been searched for in the process  $p\bar{p} \rightarrow b\bar{b}h$  ( $h \rightarrow b\bar{b}$ ). These searches excluded the large  $\tan \beta$  region ( $\tan \beta > 35$ ) not accessible at LEP [5].

In the MSSM, the charged Higgs mass at tree level,  $m_{H^\pm}$ , is related to  $m_A$  as:

$$m_{H^\pm}^2 = m_W^2 + m_A^2, \quad (2)$$

and is less sensitive to radiative corrections [7]. At LEP, the main production mechanism of the charged Higgs is  $e^+e^- \rightarrow H^+H^-$ . Direct searches of the charged Higgs at LEP have been carried in the general 2HDM (where  $m_{H^\pm}$  is not constrained) assuming  $H^+ \rightarrow \tau^+\nu_\tau$  ( $c\bar{s}$ ) and  $H^- \rightarrow \tau^-\bar{\nu}_\tau$  ( $\bar{c}s$ ). These searches yielded a lower bound of 78.6 GeV on the charged Higgs mass independent of the  $H^\pm \rightarrow \tau^\pm\nu_\tau$  branching ratio [8]. At the Tevatron, CDF and DØ performed direct and indirect searches for the charged Higgs through the process  $p\bar{p} \rightarrow t\bar{t}$ , with at least one top quark decaying via  $t \rightarrow H^\pm b$ . The direct searches seek the process  $H^\pm \rightarrow \tau^\pm\nu_\tau$  with the identification of the  $\tau$  lepton through its hadronic decays. In the indirect searches, CDF and DØ looked for a deficit in the SM  $t\bar{t}$  decays caused by the possible existence of  $t \rightarrow H^\pm b$ . These searches excluded the low and high  $\tan \beta$  regions up to  $\sim 160$  GeV [9]. Other experimental bounds on the charged Higgs mass come from processes where the charged Higgs enters as a virtual particle. One such process is the  $b \rightarrow s\gamma$  decay where indirect limits are obtained from the measurement of the decay rate [10]. However, these bounds are strongly model dependent [11, 12].

The search for the charged Higgs boson will be continued above the top quark mass. The main production mechanisms would be the  $2 \rightarrow 3$  process  $gg \rightarrow tbH^\pm$  and the  $2 \rightarrow 2$  process  $gb \rightarrow tH^\pm$  shown in Fig. 1 [13]. Additional production mechanisms come from the Drell-Yan type process  $gg, q\bar{q} \rightarrow H^+H^-$  [14], and the associated production with a  $W$  boson,  $q\bar{q} \rightarrow H^\pm W^\mp$  [15]. However, in the former case, the rate is rather low at the LHC either because of weak couplings and low quark luminosity or the process is induced by loops of heavy quarks and therefore suppressed by additional factors of electroweak couplings; in the latter case, the rate is also somewhat lower at the LHC and this channel suffers from

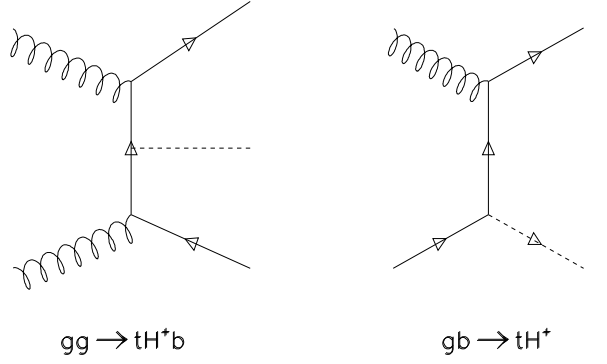


FIG. 1: The charged Higgs production at the LHC through the  $2 \rightarrow 3$  process,  $gg \rightarrow tbH^\pm$  and the  $2 \rightarrow 2$  process,  $gb \rightarrow tH^\pm$ . The inclusive cross section is the sum of both contributions after the subtraction of the common terms.

the large irreducible  $t\bar{t}$  and QCD jet backgrounds [16]. The main production mechanisms, i.e., the  $2 \rightarrow 3$  and the  $2 \rightarrow 2$  processes, partially overlap when the former is obtained from the latter by a gluon splitting into a  $b$ -quark pair. When summing both contributions, care must be taken to avoid double counting. The difference between the two processes is well understood and the inclusive cross section is obtained from a proper subtraction of the common logarithmic terms [17, 18, 19, 20]. Assuming a heavy SUSY spectrum, the charged Higgs will decay only into SM particles as shown in Fig. 2 [21] for the maximal stop mixing scenario. For low values of  $\tan \beta$ , below the top quark mass, the main decay channels are  $H^\pm \rightarrow \tau^\pm\nu_\tau$ ,  $c\bar{s}$ ,  $W^0$  and  $t^*b$ ; above the top quark mass, the  $H^\pm \rightarrow tb$  decay mode becomes dominant. For high values of  $\tan \beta$ , the  $H^\pm \rightarrow \tau^\pm\nu_\tau$  and  $H^\pm \rightarrow tb$  are the only dominant decay modes.

In this paper, we summarise the sensitivity of the ATLAS detector at the LHC to the discovery of a heavy charged Higgs, with emphasis on the region above the top quark mass,  $m_{H^\pm} > m_t$  (some of the results presented here have already been published in earlier papers [22, 23, 24, 25, 26]).

These studies have been carried out as particle level event generation in PYTHIA5.7 and PYTHIA6.1 [27], at  $\sqrt{s} = 14$  TeV, with the detector resolutions and efficiencies parameterised in ATLFast [28] from full detector simulations. We used the CTEQ2L and CTEQ5L parton distribution function parametrisations [29] and the charged Higgs mass is calculated to 1-loop with FeynHiggsFast [30].

In section II, we describe briefly the ATLAS detector and the performance of the detector components necessary for the discovery of the charged Higgs discovery. In section III, we discuss the possibility to detect the process  $H^\pm \rightarrow tb$ , followed by  $H^\pm \rightarrow \tau^\pm\nu_\tau$  in section IV. Then, we discuss the process  $H^\pm \rightarrow W^\pm h^0$  and we give the expected achievable precisions on the charged

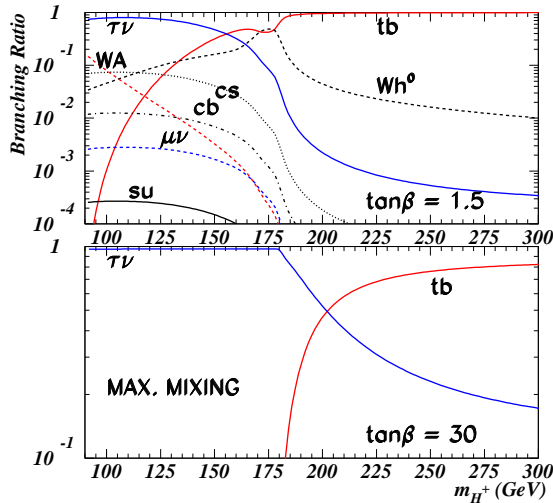


FIG. 2: The branching ratios of the charged decays in SM particles as a function of  $m_{H^\pm}$  for  $\tan\beta = 1.5$  (top plot) and  $\tan\beta = 30$  (bottom plot). The most dominant decay channels are  $H^\pm \rightarrow \tau^\pm \nu_\tau$  and  $H^\pm \rightarrow tb$ .

Higgs mass and  $\tan\beta$  determination. The detection of a charged Higgs signal in models with singlet neutrinos in large extra dimensions is discussed in section VII. Then, a discussion on charged Higgs decay to supersymmetric particles and charged Higgs production from SUSY cascade decays is presented followed by concluding remarks.

## II. DETECTOR DESCRIPTION AND PERFORMANCE

The ATLAS detector is a general purpose detector designed and optimised to be sensitive to a wide range of physics issues to be explored at the LHC such as the origin of mass at the electroweak scale. The detector itself consists of an inner detector, electromagnetic and hadronic calorimeters, a stand-alone muon spectrometer and a magnet system.

The inner detector comprises discrete high resolution semiconductor pixel and strip detectors in the inner section, and a straw tube tracking detector with the capability for transition radiation detection in the outer part. The inner detector provides pattern recognition, momentum and vertex measurements, and electron identification.

The calorimeter consists of a highly segmented electromagnetic (EM) sampling calorimeter followed by a hadronic calorimeter (HAD). The EM calorimeter is a lead/liquid argon detector with accordion shaped kapton electrodes and lead absorber plates providing electron and photon identification and measurements. This

is complemented by hermetic hadronic calorimeters for jets and missing energy measurements. The HAD covers the range  $|\eta| < 5$  with different detector technologies best suited to the variety of requirements and radiation environments. They consist of a barrel sampling detector using iron as the absorber and scintillating tiles as the active material, end-cap calorimeters with copper/liquid argon technology, and a forward calorimeter using liquid argon with rod-shaped electrodes in a tungsten matrix.

The calorimeter is surrounded by a stand-alone muon spectrometer whose design is based on the deflection of muon tracks in large super-conducting magnets. It consists of four different chamber technologies, two of which are for precision measurements of muon track parameters and the other two for triggering. In the barrel section, resistive plate chambers provide the trigger function whereas in the end-caps, this is done by thin gap chambers. Precision measurements of tracks are done with monitored drift tubes, however at large pseudo-rapidity and close to the interaction point, highly granular cathode strip chambers are used to withstand the rate and the background conditions. The muon spectrometer provides precision measurements of muon momenta and the capability for low- $p_T$  trigger at low luminosity.

The magnet system consists of a central solenoid which provides a 2 Tesla magnetic field for the inner detector, surrounded by a system of three large super-conducting air-core toroids generating the magnetic field for the muon spectrometer.

Further details on the detector design and optimisation including the trigger and data acquisition system are well documented in [31, 32]. The detection of a charged Higgs signal would depend on many crucial ATLAS detector performance parameters, namely [32, 33]:

- $\tau$ -jet reconstruction and rejection against QCD jets (for a  $\tau$ -jet reconstruction efficiency of 30%, a jet rejection factor of  $\sim 400$  can be achieved).
- Good  $E_T^{\text{miss}}$  resolution as the  $p_T^{\text{miss}}$  vector and the reconstructed  $\tau$ -jet will be used for the transverse mass reconstruction of  $H^\pm \rightarrow \tau^\pm \nu_\tau - E_T^{\text{miss}}$  resolutions of 20-100 GeV are expected based on full detector simulations of  $A/H \rightarrow \tau\tau$  events in the mass range 100-500 GeV.
- A  $b$ -tagging performance of 60% (50%) at low (high) luminosity is expected and necessary for the reconstruction  $H^\pm \rightarrow tb$  and  $H^\pm \rightarrow W^\pm h^0 \rightarrow b\bar{b}$  which contain several  $b$ -jets in the final state.
- Excellent jet reconstruction and calibration would also be needed as the reconstruction of  $W^\pm \rightarrow jj$  is necessary for the observation of the signals studied herein.
- Finally an isolated lepton ( $e$  or  $\mu$ ) trigger is needed for  $H^\pm \rightarrow tb$  and  $H^\pm \rightarrow W^\pm h^0$  and a lepton identification efficiency of 90% is expected. For the  $H^\pm \rightarrow \tau^\pm \nu_\tau$ , a multi-jet trigger (and possibly a

$\tau$  trigger) would be necessary. Such a trigger will be available, not just for the charged Higgs, but also for many other important physics studies.

The ATLFAST [28] simulation code used for the present work has been carefully verified with fully reconstructed results. Performance figures are well reproduced and we expect only slightly worse performance with the real ATLAS detector.

### III. THE $H^\pm \rightarrow tb$ CHANNEL

The region  $m_{H^\pm} > m_t$  was at first considered problematic, as the large decay mode  $H^\pm \rightarrow tb$  has large QCD backgrounds at hadron colliders. However the possibility of efficient  $b$ -tagging has considerably improved the situation [34]. The interaction term of the charged Higgs with the  $t$  and  $b$  quarks in the 2HDM of type II is given by:

$$\begin{aligned} \mathcal{L} = & \frac{g}{2\sqrt{2} m_W} V_{tb} H^+ \bar{t} (m_t \cot \beta (1 - \gamma_5) \\ & + m_b \tan \beta (1 + \gamma_5)) b + h.c. \end{aligned} \quad (3)$$

We consider therefore the large  $2 \rightarrow 2$  hadroproduction process  $gb \rightarrow tH^\pm$  (see Fig. 1) with decay mechanism  $H^\pm \rightarrow tb$ . The cross section for  $gb \rightarrow tH^\pm$  can be written as:

$$\sigma(gb \rightarrow tH^\pm) \propto m_t^2 \cot^2 \beta + m_b^2 \tan^2 \beta. \quad (4)$$

The decay width of  $H^- \rightarrow \bar{t}b$  is given by:

$$\begin{aligned} \Gamma(H^- \rightarrow \bar{t}b) \simeq & \frac{3 m_{H^\pm}}{8 \pi v^2} \left[ (m_t^2 \cot^2 \beta + m_b^2 \tan^2 \beta) \right. \\ & \times \left( 1 - \frac{m_t^2}{m_{H^\pm}^2} - \frac{m_b^2}{m_{H^\pm}^2} \right) - \frac{4 m_t^2 m_b^2}{m_{H^\pm}^2} \\ & \times \left. \left[ 1 - \left( \frac{m_t + m_b}{m_{H^\pm}} \right)^2 \right]^{1/2} \left[ 1 - \left( \frac{m_t - m_b}{m_{H^\pm}} \right)^2 \right]^{1/2} \right] \end{aligned} \quad (5)$$

where the factor 3 takes into account the number of colours. The final state of the  $2 \rightarrow 2$  hadroproduction process contains two top quarks, one of which is required to decay semi-leptonically to provide the trigger,  $t \rightarrow l\nu_b$  ( $l = e, \mu$ ) and the other hadronically,  $\bar{t} \rightarrow jjb$ . The main background comes from  $t\bar{t}b$  and  $t\bar{t}q$  production with  $t\bar{t} \rightarrow WbWb \rightarrow l\nu_b jjb$ . The rates for the signal and the backgrounds are shown in Table I.

We search for an isolated lepton, three  $b$ -tagged jets and at least two non  $b$ -jets. We retain the jet-jet combinations whose invariant masses are consistent with the  $W$ -boson mass,  $|m_W - m_{jj}| < 25$  GeV (for the events satisfying this requirement, the 4-momenta of the jets are rescaled such that  $m_{jj} = m_W$ ) and we use the  $W$ -boson mass constraint to find the longitudinal component of the neutrino momentum,  $W^\pm \rightarrow l\nu$ , assuming the missing transverse momentum is the neutrino transverse momentum. Subsequently, the two top quarks in

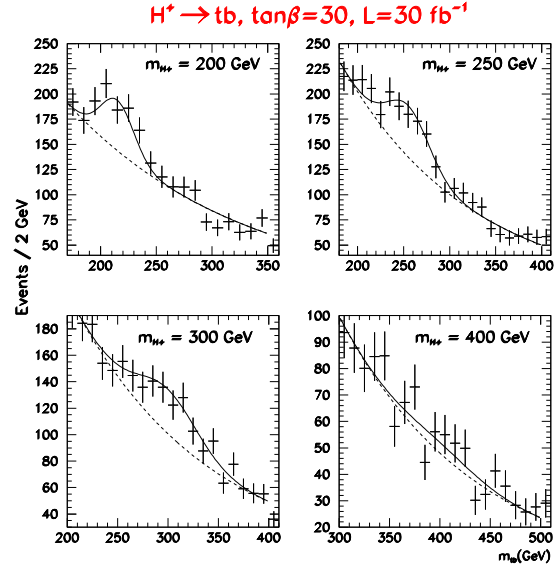


FIG. 3: The signal+background (solid line) and the background (dashed line) distributions for the reconstructed invariant mass  $m_{tb}$  of a Higgs mass of 200, 250, 300 and 400 GeV,  $\tan \beta = 30$  and an integrated luminosity of  $30 \text{ fb}^{-1}$ . The errors are statistical only.

the spectrum are reconstructed, retaining the pair of top quarks whose invariant masses  $m_{l\nu_b}$  and  $m_{jjb}$  best minimise  $\chi^2 \equiv (m_t - m_{l\nu_b})^2 + (m_t - m_{jjb})^2$ . The remaining  $b$ -jet can be paired with either top quark to give two charged Higgs candidates, one of which leads to a combinatorial background.

Above  $m_{H^\pm} = 300$  GeV, the reduced signal rate and the combinatorial background make the observation of this channel difficult. Below a charged Higgs mass of 300 GeV, this channel may be observed above the  $t\bar{t}b$  plus  $t\bar{t}q$  background. The results for  $m_{H^\pm} = 200 - 400$  GeV are shown in Fig. 3. At high values of  $\tan \beta$  ( $> 25$ ), sensitivity is expected up to 400 GeV as shown in Table II. The  $5\sigma$  discovery contour for  $H^\pm \rightarrow tb$  is shown in Fig 9. This analysis is presented extensively in [22].

### IV. THE $H^\pm \rightarrow \tau^\pm \nu_\tau$ CHANNEL

The  $\tau\nu$  decay channel offers a high  $p_T$  of the  $\tau$  and large missing energy signature that can be discovered at LHC over a vast region of the parameter space [35]. The events are generated in PYTHIA using the process  $gb \rightarrow tH^\pm$ . The associated top quark is required to decay hadronically,  $t \rightarrow jjb$ . The charged Higgs decays into a  $\tau$  lepton,  $H^\pm \rightarrow \tau^\pm \nu_\tau$ , and the hadronic decays of the  $\tau$  are considered. The backgrounds considered are QCD,  $W + \text{jets}$ , single top production  $Wt$ , and  $t\bar{t}$ , with one  $W \rightarrow jj$  and the other  $W^\pm \rightarrow \tau^\pm \nu_\tau$ . Table III shows the rates for the signal and the backgrounds as a function of  $m_{H^\pm}$  and

TABLE I: The expected rates ( $\sigma \times \text{BR}$ , in pb) — for the signal  $bg \rightarrow H^\pm t \rightarrow l\nu bjjbb$  and the  $t\bar{b} + t\bar{t}q$  background for several values of  $m_{H^\pm}$  and  $\tan \beta$ .

Process	$m_{H^\pm}$ (GeV)	$\tan \beta = 1.5$	$\tan \beta = 10$	$\tan \beta = 30$
$bg \rightarrow H^\pm t \rightarrow l\nu bjjbb$	200	3.4	0.4	1.6
	250	2.0	0.18	1.2
	300	1.2	0.14	1.0
	400	0.54	0.08	0.4
	500	0.3	0.04	0.2
$t\bar{t} \rightarrow jjbWb (W \rightarrow l\nu)$	228	228	228	

TABLE II: Sensitivity of the ATLAS detector ( $S/\sqrt{B}$ ) to the observation of the charged Higgs through  $H^\pm \rightarrow tb$ . Discovery is possible in the low ( $< 2.5$ ) and the high ( $> 25$ )  $\tan \beta$  regions up to 400 GeV

$m_{H^\pm}$ (GeV)	$\tan \beta = 1$	$\tan \beta = 2$	$\tan \beta = 10$	$\tan \beta = 25$	$\tan \beta = 35$
200	11.5	5.3	1.3	2.9	5.5
250	19.6	6.1	1.1	5.1	11.1
300	13.8	5.2	1.1	4.9	9.9
400	7.7	2.8	0.5	2.3	4.7

$\tan \beta$ .

The width of the process  $H^\pm \rightarrow \tau^\pm \nu_\tau$  is:

$$\Gamma(H^\pm \rightarrow \tau^\pm \nu_\tau) \simeq \frac{m_{H^\pm}}{8\pi v^2} \left[ m_\tau^2 \tan^2 \beta \right. \\ \times \left. \left( 1 - \frac{m_\tau^2}{m_{H^\pm}^2} \right) \right] \left( 1 - \frac{m_\tau^2}{m_{H^\pm}^2} \right). \quad (6)$$

If the decay  $H^\pm \rightarrow tb$  is kinematically allowed, comparing (6) with (5) one can have a rough estimate of the  $H^\pm \rightarrow \tau^\pm \nu_\tau$  branching ratio  $BR_\tau$ :

$$BR_\tau \simeq \frac{\Gamma(H^\pm \rightarrow \tau^\pm \nu_\tau)}{\Gamma(H^\pm \rightarrow tb) + \Gamma(H^\pm \rightarrow \tau^\pm \nu_\tau)} \\ = \frac{m_\tau^2 \tan^2 \beta}{3(m_t^2 \cot^2 \beta + m_b^2 \tan^2 \beta) + m_\tau^2 \tan^2 \beta}. \quad (7)$$

A measurement of the signal rate in  $H^\pm \rightarrow \tau^\pm \nu_\tau$  can allow a determination of  $\tan \beta$  (see section VIC for details).

The distributions of one-prong hadronic decays of  $\tau$ 's,

$$\begin{aligned} \tau^\pm &\rightarrow \pi^\pm \nu_\tau & (11.1\%) \\ \tau^\pm &\rightarrow \rho^\pm (\rightarrow \pi^\pm \pi^0) \nu_\tau & (25.2\%) \\ \tau^\pm &\rightarrow a_1^\pm (\rightarrow \pi^\pm \pi^0 \pi^0) \nu_\tau & (9.0\%), \end{aligned} \quad (8)$$

are sensitive to the polarisation state of the  $\tau$  lepton [36, 37, 38]. In fact, it is to be noted that the spin state of  $\tau$ 's coming from  $H^\pm$ - and  $W^\pm$ -boson decays are opposite as illustrated in Fig. 6. This is true for the case of one-prong decays into both  $\pi^\pm$ 's and longitudinal vector mesons, while the transverse component of the latter dilutes the effect and must be somehow eliminated by requiring that 80% of the  $\tau$ -jet (transverse) energy is carried away by the  $\pi^\pm$ 's, i.e.:

$$R = \frac{p_T^{\pi^\pm}}{p_T^\tau} > 0.8. \quad (9)$$

Alternatively, one can demand a hard distribution in  $\Delta p_T$  which is the difference in the momenta of the charged track and the accompanying neutral pion(s) [36],

$$\Delta p_T = |p_T^{\pi^\pm} - p_T^{\pi^0}|. \quad (10)$$

Ultimately, the polarisation effect leads to a significantly harder momentum distribution of charged pions from  $\tau$  decays for the  $H^\pm$  signal compared to the  $W^\pm$  background, which can then be exploited to increase the signal-to-background ratios and the signal significances [36, 37, 38] by reducing the background and enhancing the signal [23]. We have included the  $\tau$  polarisation into PYTHIA through the TAUOLA [39] simulation code and considered all the hadronic decays of the  $\tau$  lepton.

We search for one hadronic  $\tau$  jet and at least three non  $\tau$  jets, one of which must be a  $b$ -tagged jet. Further, we apply a  $b$ -jet veto to reject the  $t\bar{t}$  background. As there is no isolated lepton (electron or muon) in the final state, the observation of this channel requires a multi-jet trigger with a  $\tau$  trigger. After reconstructing the jet-jet invariant mass  $m_{jj}$  and retaining the candidates consistent with the  $W$ -boson mass, the jet 4-momenta are rescaled as done in the  $H^\pm \rightarrow tb$  analysis and the associated top quark is reconstructed by minimising  $\chi^2 = (m_{jjb} - m_t)^2$ . Subsequently, a sufficiently high threshold on the  $p_T$  of the  $\tau$  jet is required. The background events satisfying this cut need a large boost from the  $W$  boson. This results in a small azimuthal opening angle  $\Delta\phi$  between the  $\tau$  jet and the missing momentum  $\not{p}_T$ . In contrast, such a boost is not required from the  $H^\pm$  for the signal events, leading to a backward peak in the azimuthal opening angle [23]. Furthermore, the missing momentum is harder for the signal. The difference between signal and background distributions in the azimuthal angle and the missing momentum increases with increasing  $m_{H^\pm}$ .

TABLE III: The expected rates ( $\sigma \times BR$ ), for the signal  $gb \rightarrow tH^\pm$  with  $H^\pm \rightarrow \tau^\pm \nu_\tau$  and  $t \rightarrow jjb$ , and for the backgrounds: QCD,  $W+jets$ ,  $Wtb$  and  $t\bar{t}$  with  $t \rightarrow \tau\nu b$  and  $\bar{t} \rightarrow jjb$ . We assume an inclusive  $t\bar{t}$  production cross section of 590 pb. Other cross sections are taken from PYTHIA. The branching fractions of  $H^\pm \rightarrow \tau^\pm \nu_\tau$  are obtained from HDECAY [21], and we take the  $W \rightarrow jj$  branching ratio to be 2/3.

Process	$\tan \beta$	$m_{H^\pm}$ (GeV)	$\sigma \times BR$ (pb)
Signal	15	180	1.33
	30	200	2.23
	40	250	0.91
	45	300	0.54
	25	350	0.10
	35	400	0.13
	60	450	0.23
$t\bar{t}$	50	500	0.11
			84.11
			56.9
			$1.64 \cdot 10^4$
$Wt$ ( $p_T > 30$ GeV)			$6.04 \cdot 10^9$
$W+jets$ ( $p_T > 30$ GeV)			
QCD ( $p_T > 10$ GeV)			

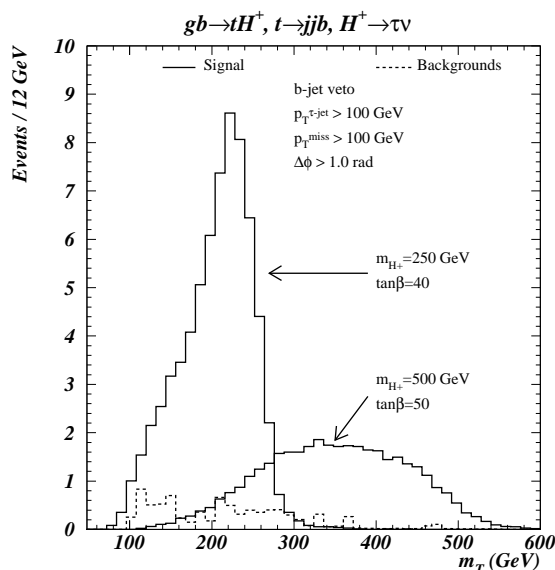


FIG. 4: The final transverse mass  $m_T$  reconstruction for the signal and the backgrounds taking into account the polarisation of the  $\tau$  lepton, for an integrated luminosity of  $30 \text{ fb}^{-1}$ .

These effects are well cumulated in the transverse mass

$$m_T = \sqrt{2p_T^\tau p_T [1 - \cos(\Delta\phi)]}, \quad (11)$$

which provides a good discrimination between the signal and the backgrounds as shown in Fig 4 — the full invariant mass is not reconstructed in this case because of the neutrino in the final state. For the backgrounds, the transverse mass is kinematically constrained to be smaller than  $m_W$  but for the signal, the transverse mass is bound from above by  $m_{H^\pm}$ . However, because of the

experimental resolution of  $E_T^{\text{miss}}$ , some leakage of the background events into the signal region is observed (see Fig. 4). The backgrounds in this channel are relatively small; significances upwards of  $5\sigma$  can be achieved for  $m_{H^\pm} > m_t$  and  $\tan \beta > 10$ , for an integrated luminosity of  $30 \text{ fb}^{-1}$  as shown in Table IV. The discovery contour for this channel is shown in Fig. 9. In fact, the range of discovery potential is solely limited by the signal size itself. The present study shows a statistically significant improvement in the signal-to-background ratios and in the signal significances due to the  $\tau$  polarisation effect but it is not necessary to restrict oneself to just the one-prong decays. Details of this study are available in [23].

## V. THE $H^\pm \rightarrow W^\pm h^0$ CHANNEL

Thus far, the study of the discovery potential of the charged Higgs with ATLAS has concentrated mainly on the fermionic decay modes —  $H^\pm \rightarrow tb$  and  $H^\pm \rightarrow \tau^\pm \nu_\tau$  [22, 23, 40]. In this section, the discovery potential of the charged Higgs with the ATLAS detector through the process  $H^\pm \rightarrow W^\pm h^0$  is studied. The decay width of  $H^- \rightarrow W^- h^0$  is:

$$\Gamma(H^- \rightarrow W^- h^0) \simeq \frac{\cos^2(\beta - \alpha)}{16 \pi v^2} \times \left[ 1 - \left( \frac{m_h + m_W}{m_{H^\pm}} \right)^2 \right]^{1/2} \left[ 1 - \left( \frac{m_h - m_W}{m_{H^\pm}} \right)^2 \right]^{1/2} \quad (12)$$

where  $\alpha$  is the Higgs mixing angle in the CP-even sector. In the MSSM one can easily verify that the maximum value of  $\cos^2(\beta - \alpha)$  at fixed  $\tan \beta$  is  $\cos^2 2\beta$  and occurs in the limit  $m_{H^\pm} \rightarrow m_W$ . Therefore the expectation of a heavy charged Higgs implies a small coupling for this channel. Though significant only in a tiny range of MSSM parameter space [41], this channel constitutes a

TABLE IV: The expected signal-to-background ratios and significances calculated after all cuts for an integrated luminosity of  $30 \text{ fb}^{-1}$ . The backgrounds are relatively small; in fact, it is the size of the signal itself that limits the range of the discovery potential.

$\tan \beta$	30	40	45	25	35	60	50
$m_{H^\pm}$ (GeV)	200	250	300	350	400	450	500
Signal events	46.3	60.3	70.5	18.8	30.6	66.9	36.2
$t\bar{t}$	3.1	3.1	3.1	3.1	3.1	3.1	3.1
$Wt$	3.2	3.2	3.2	3.2	3.2	3.2	3.2
$W+\text{jets}$	0.3	0.3	0.3	0.3	0.3	0.3	0.3
Total background	6.7	6.7	6.7	6.7	6.7	6.7	6.7
$S/B$	6.9	9.0	10.5	2.8	4.6	10.0	5.4
$S/\sqrt{B}$	17.9	23.3	27.2	7.3	11.8	25.8	14.0

unique test for the MSSM and is also sensitive to the next-to-minimal extension to the MSSM, i.e., NMSSM, where there may be a significant range of viability below and above the top quark mass [42].

### A. $H^\pm \rightarrow W^* h^0$ , $m_{H^\pm} < m_t$

Below the top quark mass, we consider  $t\bar{t}$  production with one top quark decaying into a  $W$  boson and the other into the charged Higgs. The characteristics of the production and decay processes are:

$$\begin{aligned} gg(q\bar{q}) &\rightarrow t\bar{t} \\ t &\rightarrow H^\pm b \\ \bar{t} &\rightarrow W\bar{b} \\ H^\pm &\rightarrow W^* h^0. \end{aligned} \quad (13)$$

Thus, the spectrum contains two  $W$  bosons, one of which is off mass shell, and four  $b$ -quarks due to the subsequent decay  $h^0 \rightarrow b\bar{b}$ . In the present analysis, one of the  $W$ 's is required to decay into leptons ( $e, \mu$ ), and the other into jets. The major background to this process comes from  $t\bar{t}b\bar{b}$  and  $t\bar{t}q\bar{q}$  production where both top quarks decay into  $W$ 's. We search for an isolated lepton, four  $b$ -tagged jets and at least two non  $b$ -jets. Two possible scenarios are considered on an event by event basis:

$$W^* \rightarrow l\nu \quad W \rightarrow jj \quad (14)$$

or

$$W^* \rightarrow jj \quad W \rightarrow l\nu. \quad (15)$$

If the on-shell  $W$  boson decays into leptons, then the  $W$  mass constraint is used to fix the longitudinal component  $p_L^\nu$  of the neutrino momentum. For this case,  $W^* \rightarrow jj$  and all the jet-jet combinations are accepted. However, if  $W^* \rightarrow l\nu$  instead, one can no longer use the  $W$  mass constraint. In this case,  $p_L^\nu$  is set to zero and the jet-jet combinations consistent with the  $W$  mass are retained, i.e.,  $|m_W - m_{jj}| < 25 \text{ GeV}$ ; in this mass window, the jet momenta are rescaled so that  $m_{jj} = m_W$ . Finally, we use the following  $\chi^2$  criterion to select the best top quark,

the neutral light Higgs and charged Higgs candidates:

$$\begin{aligned} \chi^2 = & (m_{Wb_i} - m_t)^2 + (m_{H^\pm b_i} - m_t)^2 \\ & + (m_{b_j b_k} - m_{h^0})^2. \end{aligned} \quad (16)$$

Although the signal rate is initially two orders of magnitude smaller than the  $t\bar{t}$  background rate as can be seen from Table V, the proposed reconstruction procedure described in further detail in [24] permits the extraction of the signal with a significance exceeding  $5\sigma$  in the low  $\tan \beta$  ( $1.5 - 2.5$ ) region as shown in Table VI. At high  $\tan \beta$ , though the reconstruction efficiency remains comparable, the signal rate decreases so significantly that the discovery potential vanishes in this region.

### B. $H^\pm \rightarrow W^\pm h^0$ , $m_{H^\pm} > m_t$

Above the top quark mass, the charged Higgs is produced in association with a top quark according to:

$$\begin{aligned} gb &\rightarrow tH^\pm \\ H^\pm &\rightarrow Wh^0 \\ t &\rightarrow Wb. \end{aligned} \quad (17)$$

The final state for the signal contains two  $W$  bosons, one of which is required to decay into leptons (electron or muon to trigger the experiment), the other into jets, and three  $b$ -jets due to the subsequent decay  $h^0 \rightarrow b\bar{b}$ . The background in this case comes from  $t\bar{t}b$  and  $t\bar{t}q$  events with both top quarks decaying into  $W$ 's. We search for one isolated lepton, three  $b$ -tagged jets and at least two non  $b$ -jets. In this case, both  $W$ -bosons are on the mass shell. The  $W$  mass constraint is used to find a longitudinal component of the neutrino momentum,  $W^\pm \rightarrow l\nu$ , and the jet-jet combinations satisfying the requirement  $|m_{jj} - m_W| < 25 \text{ GeV}$  are retained as done in the previous analysis. The associated top quark from  $gb \rightarrow tH^\pm$ ,  $t \rightarrow Wb$  and the neutral light Higgs,  $h^0 \rightarrow b\bar{b}$  are reconstructed by minimising  $\chi^2 = (m_{Wb_i} - m_t)^2 + (m_{b_i b_m} - m_{h^0})^2$ . Initially, the total background is at least three orders of magnitude higher than the signal in the most favourable case ( $\tan \beta = 3$ ), as shown in Table VII. However, with the

TABLE V: The expected rates ( $\sigma \times BR$ ) for the signal  $t\bar{t} \rightarrow bH^\pm Wb$  with  $H^\pm \rightarrow W^*h^0$  and for the  $t\bar{t}$  backgrounds. It should be noted that due to the  $\tan\beta$  dependence of the  $t \rightarrow H^\pm b$  and of the  $t \rightarrow Wb$  branching ratios, the  $t\bar{t}$  background rates depend on  $\tan\beta$ .

Process	$\tan\beta$	$m_{h^0}$ (GeV)	$m_{H^\pm}$ (GeV)	$\sigma \times$	BR (pb)
$H^\pm \rightarrow W^*h^0$	2.0	83.5	152	1.2	
	3.0	93.1	152		0.2
$t\bar{t} \rightarrow jjbl\nu b$	2.0			143	
	3.0				152

TABLE VI: The expected signal-to-background ratios and significances for an integrated luminosity of  $300 \text{ fb}^{-1}$ .  $\langle m_t \rangle$ ,  $\langle m_{H^\pm} \rangle$  and  $\langle m_{h^0} \rangle$  are the means of the Gaussian fits to the distributions of  $m_{H^\pm b}$ ,  $m_{W^*h^0}$  and  $m_{b\bar{b}}$  respectively. The nominal values are shown in Table V for  $m_{H^\pm}$  and  $m_{h^0}$ . A central value of 175 GeV is taken for the top quark mass.  $m_{H^\pm}$  and  $m_t$  are not reconstructed at their nominal values (within the large statistical uncertainties, the numbers are consistent with the nominal values): this is due to the assumption that  $p_L^\nu = 0$  (made in selection cuts) and also to the fact that the 4-momentum of the  $W^*$  in  $H^\pm \rightarrow W^*h^0$  and  $t \rightarrow W^*h^0b$  is not rescaled to the  $W$  mass before reconstructing the charged Higgs and the top quark. The other top quark is reconstructed to the nominal value (see [24] for details) since here,  $t \rightarrow Wb$ ; this  $W$  boson is on-shell: in the leptonic channel the  $W$  mass constraint guarantees that  $m_{l\nu} = m_W$ , and in the hadronic channel, the jet momenta are rescaled within a mass window so that  $m_{jj} = m_W$ . The significances and the signal-to-background ratios are calculated within  $\pm 2\sigma_{H^\pm}$  of  $\langle m_{H^\pm} \rangle$ .

	$\tan\beta = 2$	$\tan\beta = 3$
$\langle m_t \rangle$ (GeV)	$188 \pm 20$	$190 \pm 29$
$\sigma_t$ (GeV)	$18 \pm 11$	$20 \pm 10$
$\langle m_{H^\pm} \rangle$ (GeV)	$157 \pm 7$	$160 \pm 10$
$\sigma_{H^\pm}$ (GeV)	$19 \pm 8$	$21 \pm 10$
$\langle m_{h^0} \rangle$ (GeV)	$83 \pm 1$	$92 \pm 4$
$\sigma_{h^0}$ (GeV)	$12 \pm 1$	$13 \pm 3$
Signal events	136	25
Background events	40	43
$S/B$	3.4	0.6
$S/\sqrt{B}$	21.5	3.8

reconstruction technique described in detail in [24], the signal-to-background ratios could be improved by two orders of magnitude. This improvement is still insufficient to observe the signal over the background; for example, for  $\tan\beta = 3$  and  $m_{H^\pm} = 200$  GeV, a significance of only 3.3 can be expected after 3 years at high luminosity. A parton level study of this channel was carried out in [43] using  $gg \rightarrow tbH^\pm$  and a viable signal survives above the main irreducible  $tbW^\pm h^0$  continuum for  $\tan\beta \sim 2 - 3$  and  $m_{H^\pm} \sim 200$  GeV, in fair agreement with the current analysis.

The main objective of this study is to demonstrate a good signal reconstruction and a high background suppression with the ATLAS detector. Indeed, although the signal is marginally viable in MSSM, the results can be normalised to other models, for instance NMSSM, where LEP constraints no longer apply and the discovery po-

tential in this channel would extend to a significant area of the parameter space as explained below.

### C. $H^\pm \rightarrow W^\pm h^0$ in NMSSM

In the NMSSM, the relation (2) and the direct lower limit on the CP-odd Higgs boson mass from LEP (see the introduction section) translate into an indirect lower bound on the charged Higgs,  $m_{H^\pm} \gtrsim 120$  GeV; in fact for  $\tan\beta \sim 3$ ,  $m_{H^\pm} \gtrsim 250$  GeV [3, 42]. As a result, the channel  $H^\pm \rightarrow W^\pm h^0$  has a high threshold in the LEP allowed region where the branching ration is very small (see Fig. 2). Indeed, beyond  $\tan\beta = 3$ , as demonstrated by the study shown here, this channel presents no discovery potential due to the very low signal rate. It has been argued that in the singlet extension to MSSM,

TABLE VII: The rates for the signal  $bg \rightarrow H^\pm t \rightarrow Wh^0 Wb$  and the  $t\bar{t}$  background as a function of  $\tan\beta$ .

Process	$\tan\beta$	$m_{h^0}$ (GeV)	$m_{H^\pm}$ (GeV)	$\sigma \times$	BR (pb)
$H^\pm \rightarrow W^\pm h^0$	1.5	78.0	250	0.023	
	3.0	99.1	200	0.134	
	5.0	104.9	200	0.031	
$t\bar{t} \rightarrow jjbl\nu b$					228

i.e., NMSSM, this channel is immune to the LEP constraints and there may be a significant discovery potential above and below the top quark mass [42]. In fact, NMSSM extends the Higgs sector of the MSSM by adding a complex singlet scalar field and seven physical Higgs bosons are predicted in this model, three neutral CP-even  $h^0$ ,  $H_1^0$ , and  $H_2^0$ , two CP-odd  $A_1^0$  and  $A_2^0$ , and a charged pair  $H^\pm$  [1]. The parameter space is therefore less constrained than the one of the MSSM and the indirect lower limits on the Higgs masses from LEP are no longer valid. In addition, the mixing between the singlet and the doublet states would dilute the direct mass limits on the latter from LEP. Consequently, the channel  $H^\pm \rightarrow W^\pm (h^0, A^0)$  can be the dominant decay mode for low  $\tan\beta$  and  $m_{H^\pm} \sim 160$  GeV. Therefore, The  $H^\pm \rightarrow W^\pm h^0$  channel which is marginally viable in MSSM would yield a significant signal in NMSSM [42].

## VI. $m_{H^\pm}$ AND $\tan\beta$ DETERMINATION

In this section, we discuss the expected precisions on the charged Higgs mass and  $\tan\beta$  measurements with the ATLAS detector in the  $H^\pm \rightarrow tb$  and  $H^\pm \rightarrow \tau^\pm \nu_\tau$  channels.

### A. $H^\pm$ mass determination in $H^\pm \rightarrow \tau^\pm \nu_\tau$

As discussed in section IV, this channel does not offer the possibility for the observation of a resonance peak above the background, only the transverse Higgs mass can be reconstructed because of the presence of the neutrino in the final state. The background comes from single top ( $Wt$ ) and  $t\bar{t}$  productions with one  $W^\pm \rightarrow \tau^\pm \nu_\tau$ . Thus, the transverse mass is kinematically constrained to be less than the  $W$ -boson mass while in the signal, the upper bound is the charged Higgs mass.

The differences in the event topology and in the  $\tau$  polarisation have been used to suppress the backgrounds as discussed in section IV [23, 44], so that above the  $W$  mass threshold, the background in this channel is relatively small as shown in Fig. 4. As a result, although there is no reconstruction of the resonance peak in this channel, the Higgs mass can be extracted from the transverse mass distribution with a relatively good precision.

For the mass determination in this channel, we use the likelihood method presented in [25, 45].

Three main sources of systematic uncertainties are included in the mass determination: the shape of the background, the background rate and the energy scale. The background shape becomes more significant at lower Higgs masses where there is more overlap between signal and background. To include this effect, we assumed a linear variation of the background shape, from  $-10\%$  to  $+10\%$  between the minimum and the maximum of the transverse mass distribution. Another source of systematic uncertainty is the rate of the backgrounds. It is expected that the background rate ( $Wt$  and  $t\bar{t}$ ) could be known to  $5\%$  [45]. Therefore, to take this effect into account, we increase the background rate by  $5\%$  while at the same time we decrease the signal by  $5\%$ . Finally, we also include the scale uncertainty:  $1\%$  for jets and  $0.1\%$  for photons, electrons and muons. In Table VIII, we show the effects of the systematic uncertainties: the overall uncertainty in the mass determination is dominated by statistics.

The overall relative precision in this channel ranges from  $1.3\%$  at  $m_{H^\pm} = 226$  GeV to  $3.1\%$  at  $m_{H^\pm} = 511$  GeV for an integrated luminosity of  $100 \text{ fb}^{-1}$ . At  $300 \text{ fb}^{-1}$ , the precision improves to  $0.8\%$  at  $m_{H^\pm} = 226$  GeV and  $1.8\%$  at  $m_{H^\pm} = 511$  GeV [25].

### B. $H^\pm$ Mass Determination in $H^\pm \rightarrow tb$

In the  $tb$  channel, the full invariant mass can be reconstructed as shown in Fig. 3 although this channel suffers from the large irreducible  $t\bar{t}b$  background and also from the signal combinatorial background. The determination of the mass can be done using the likelihood method described in [25, 45] or by fitting the signal and the background. In the latter case, one assumes that the background shape and normalisation can be determined by fitting outside the signal region, thus, the systematic uncertainties include only the scale uncertainty. We assume a Gaussian shape for the signal and an exponential for the background and fit signal+background including the statistical fluctuations and the scale uncertainty. The precisions on the mass determination from the likelihood and fitting methods are comparable.

The relative precision in this channel ranges from  $0.8\%$  at  $m_{H^\pm} = 226$  GeV to  $5.2\%$  at  $m_{H^\pm} = 462$  GeV for

TABLE VIII: The systematic effects on the mass determination in the  $H^\pm \rightarrow \tau^\pm \nu_\tau$  channel are small. Columns 2 and 3 show the statistical uncertainties for an integrated luminosity of  $300 \text{ fb}^{-1}$ . Columns 4 and 5 include the systematic uncertainties. The total uncertainties are dominated by the statistical errors.

$m_{H^\pm}$ (GeV)	Statistics only		With systematics	
	$\langle m \rangle$	$\delta m$	$\langle m \rangle$	$\delta m$
225.9	226.4	1.7	225.9	1.7
271.1	271.1	2.0	270.9	2.3
317.8	318.3	3.0	319.9	3.5
365.4	365.7	4.6	365.2	4.7
413.5	413.8	4.5	414.9	4.7
462.1	462.6	6.0	460.8	6.3
510.9	511.9	7.4	511.7	9.2

$100 \text{ fb}^{-1}$ . For  $300 \text{ fb}^{-1}$ , the precision improves to 0.5% at 226 GeV and 3.5% at 462 GeV [25].

### C. Determination of $\tan \beta$

It is possible to determine  $\tan \beta$  by measuring the signal rate in the  $\tau \nu$  channel where the backgrounds are relatively low. The main systematic error would come from the knowledge of the luminosity. The uncertainty in the rate measurement can be estimated as [46]:

$$\frac{\Delta(\sigma \times BR)}{\sigma \times BR} = \sqrt{\frac{S+B}{S^2} + \left(\frac{\Delta \mathcal{L}}{\mathcal{L}}\right)^2}, \quad (18)$$

where the relative uncertainty on the luminosity measurement is taken conservatively to be 10%. The uncertainty on  $\tan \beta$  is computed as:

$$\Delta \tan \beta \simeq \Delta(\sigma \times BR) \left[ \frac{d(\sigma \times BR)}{d \tan \beta} \right]^{-1}. \quad (19)$$

At large  $\tan \beta$ , from Equations (4) and (7), the rate in the  $H^\pm \rightarrow \tau^\pm \nu_\tau$  channel is obtained as:

$$\sigma \times BR \propto \tan^2 \beta. \quad (20)$$

From the relations (19) and (20), we get:

$$\frac{\Delta \tan \beta}{\tan \beta} = \frac{1}{2} \frac{\Delta(\sigma \times BR)}{\sigma \times BR}. \quad (21)$$

The relative precision on  $\tan \beta$  ranges from 15.4% to 7.3% for  $\tan \beta = 20$  to 50, at low luminosity. For an integrated luminosity of  $300 \text{ fb}^{-1}$ , the precision improves to 7.4% at  $\tan \beta = 20$  and to 5.4% at  $\tan \beta = 50$  [25].

Fig. 5 illustrates the expected overall precision on the charged Higgs mass and  $\tan \beta$  determination for an integrated luminosity of  $300 \text{ fb}^{-1}$ . In either channel, the overall uncertainties are dominated by the statistical errors. The  $\tau \nu$  channel offers better precisions on the Higgs

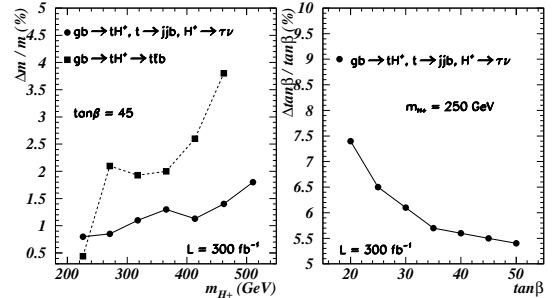


FIG. 5: The expected overall precision on the charged Higgs mass and on  $\tan \beta$  measurements, as a function of the charged Higgs mass (left plot) and  $\tan \beta$  (right plot) respectively. For the mass determination, the  $H^\pm \rightarrow \tau^\pm \nu_\tau$  channel gives better precisions than  $H^\pm \rightarrow tb$  except at low Higgs masses. In addition,  $H^\pm \rightarrow \tau^\pm \nu_\tau$  allows for the determination of  $\tan \beta$  by measuring the rate in this channel.

mass determination than the  $tb$  channel, except at low Higgs masses where the  $\tau \nu$  channel suffers from a much reduced selection efficiency or a much higher background level as shown in Table IX and Fig. 5 [25].

## VII. $H^\pm \rightarrow \tau^\pm \nu_\tau$ IN LARGE EXTRA DIMENSIONS

In models where extra dimensions open up at the TeV scale, small neutrino masses can be generated without implementing the seesaw mechanism [47, 48, 49]. These models postulate the existence of  $\delta$  additional spatial dimensions of size  $R$  where gravity and perhaps other fields freely propagate while the SM degrees of freedom are confined to (3+1)-dimensional wall (4D) of the higher dimensional space. The idea that our world could be a topological defect of a higher-dimensional theory [50] finds a natural environment in string theory [51].

TABLE IX: The overall precisions on the mass determination are better in the  $\tau\nu$  channel than in the  $tb$  channel. This is due to the fact that the latter suffers from large  $t\bar{t}b$  and signal combinatorial backgrounds ( $\mathcal{L} = 100 \text{ fb}^{-1}$ ).

$m_{H^\pm}$ (GeV)	$H^\pm \rightarrow \tau^\pm \nu_\tau$		$H^\pm \rightarrow tb$	
	$\langle m \rangle$	$\delta m$	$\langle m \rangle$	$\delta m$
225.9	225.9	2.9	226.9	1.8
271.1	271.0	3.9	270.1	10.1
317.8	319.7	5.9	320.2	11.3
365.4	364.9	8.1	365.4	12.1
413.5	414.8	8.0	417.4	17.6
462.1	460.7	10.6	465.9	24.1
510.9	511.4	15.7		

The right-handed neutrino can be interpreted as a singlet with no quantum numbers to constrain it to the SM brane and thus, it can propagate into the extra dimensions just like gravity [52]. Such singlet states in the bulk couple to the SM states on the brane as right-handed neutrinos with small couplings — the Yukawa couplings of the bulk fields are suppressed by the volume of the extra dimensions. The interactions between the bulk neutrino and the wall fields generate Dirac mass terms between the wall fields and all the Kaluza-Klein modes of the bulk neutrino. As long as this mass is less than  $1/R$ , the Kaluza-Klein modes are unaffected while for the zero mode, the interaction generates a Dirac neutrino mass suppressed by the size of the extra dimensions:

$$m_D = \frac{\lambda}{\sqrt{2}} \frac{M_*}{M_{Pl}} v \quad (22)$$

where  $\lambda$  is a dimensionless constant,  $v$  the Higgs vacuum expectation value (see the introduction section),  $M_{Pl} = 2.4 \times 10^{18} \text{ GeV}$  is the reduced Planck scale related to the usual Planck mass  $1.2 \times 10^{19} \text{ GeV} = \sqrt{8\pi} M_{Pl}$ , and  $M_*$  is the true scale of gravity, or the fundamental Planck scale of the  $(4+\delta)\text{D}$  space time:

$$M_{Pl}^2 = R^\delta M_*^{\delta+2}. \quad (23)$$

The mixing between the lightest neutrino with mass  $m_D$  and the heavier neutrinos introduces a correction  $N$  to the Dirac mass such that the physical neutrino mass  $m_\nu$  is [49]:

$$m_\nu = \frac{m_D}{N}, \quad (24)$$

where

$$N \simeq 1 + \left( \frac{m_D}{M_*} \right)^2 \left( \frac{M_{Pl}}{M_*} \right)^2 \frac{2\pi^{\delta/2}}{\Gamma(\delta/2)} \frac{1}{\delta-2}. \quad (25)$$

As shown in Table X, small neutrino masses,  $m_\nu$ , can be obtained consistent with atmospheric neutrino oscillations [53].

$H^-$  decays to the right-handed  $\tau^-$  through the  $\tau$  Yukawa coupling:

$$H^- \rightarrow \tau_R^- \bar{\nu}. \quad (26)$$

The  $H^-$  decay to left-handed  $\tau^-$  is completely suppressed in MSSM. However, in the scenario of singlet neutrino in large extra dimensions,  $H^-$  can decay to both right-handed and left-handed  $\tau^-$  depending on the parameters  $M_*$ ,  $m_D$ ,  $\delta$ ,  $m_{H^\pm}$  and  $\tan\beta$  (see [26] for detailed formulas):

$$H^- \rightarrow \tau_L^- \bar{\nu} + \tau_R^- \psi, \quad (27)$$

where  $\psi$  is a bulk neutrino and  $\nu$  is dominantly a light neutrino with a small admixture of the Kaluza-Klein modes. The measurement of the polarisation asymmetry,

$$A = \frac{\Gamma(H^- \rightarrow \tau_L^- \psi) - \Gamma(H^- \rightarrow \tau_R^- \bar{\nu})}{\Gamma(H^- \rightarrow \tau_L^- \psi) + \Gamma(H^- \rightarrow \tau_R^- \bar{\nu})}, \quad (28)$$

can be used to distinguish between the ordinary 2HDM-II and the scenario of singlet neutrino in large extra dimensions. In the 2HDM-II, the polarisation asymmetry would be  $-1.0$ . In the framework of large extra dimensions, the polarisation asymmetry can vary from  $+1$  to  $-1$ . In the latter case, the decay of  $H^-$  is similar to the 2HDM-II but possibly with a different phase space since the neutrino contains some admixture of the Kaluza-Klein modes. The singlet neutrino may not necessarily propagate into the  $\delta$ -extra dimensional space. It is possible to postulate that the singlet neutrino propagate into a subset  $\delta_\nu$  ( $\delta_\nu \leq \delta$ ) of the  $\delta$  additional spatial dimensions, in which case the formalism for the generation of small Dirac neutrino masses is merely a generalisation of the case  $\delta_\nu = \delta$  discussed above [48].

The charged Higgs decay to right-handed  $\tau$ ,  $H^- \rightarrow \tau_R^- \bar{\nu}$  have been extensively studied for the LHC as discussed above [23, 44]. In this section, we discuss the possibility to observe  $H^- \rightarrow \tau_L^- \psi$  at the LHC above the top quark mass [26, 54]. Table X shows the parameters selected for the current analysis. The cases where

TABLE X: The parameters used in the current analysis of the signal with the corresponding polarisation asymmetry. In general,  $H^-$  would decay to  $\tau_L^-$  and  $\tau_R^-$ ,  $H^- \rightarrow \tau_R^- \bar{\nu} + \tau_L^- \psi$ , depending on the asymmetry. For the decay  $H^- \rightarrow \tau_R^- \bar{\nu}$  (as in MSSM), the asymmetry is  $-1$  and this case is already studied for the LHC [23, 44] and discussed in section IV. The signal to be studied is  $H^- \rightarrow \tau_L^- \psi$ .

	$M_*$ (TeV)	$\delta_\nu$	$\delta$	$m_D$ (eV)	$m_{H^\pm}$ (GeV)	$\tan \beta$	Asymmetry	$m_\nu$ (eV)
Signal-1	2	4	4	3.0	219.9	30	$\sim 1$	$0.5 \cdot 10^{-3}$
Signal-2	20	3	3	145.0	365.4	45	$\sim 1$	0.05
Signal-3	1	5	6	5.0	506.2	4	$\sim 1$	0.05
Signal-4	100	6	6	0.005	250.2	35	$\sim -1$	0.005
Signal-5	10	4	5	0.1	350.0	20	$\sim -1$	0.04
Signal-6	50	5	5	0.04	450.0	25	$\sim -1$	0.04

the asymmetry is  $+1$  are discussed. No additional Higgs bosons are needed. As a result, the charged Higgs production mechanisms are the same as in the 2HDM-II as shown in Fig. 1. We consider the  $2 \rightarrow 2$  production process where the charged Higgs is produced with a top quark,  $gb \rightarrow tbH^\pm$ . Further, we require the hadronic decay of the top quark,  $t \rightarrow Wb \rightarrow jjb$  and the charged Higgs decay to  $\tau$  leptons.

The major backgrounds are the single top production  $gb \rightarrow Wt$ , and  $t\bar{t}$  production with one  $W^+ \rightarrow jj$  and the other  $W^- \rightarrow \tau_L^- \bar{\nu}$  (there is no enhancement in the background rate from the contribution  $W^- \rightarrow \tau_L^- \psi$ ). Depending on the polarisation asymmetry — Equation (28) —  $H^- \rightarrow \tau_R^- \bar{\nu}$  will contribute as an additional background. In Table XI, we list the rates for the signal and for the backgrounds.

In general,  $H^- \rightarrow \tau_L^- \psi + \tau_R^- \bar{\nu}$  with the asymmetry between  $-1$  and  $1$  [54]. However, the study of  $H^- \rightarrow \tau_R^- \bar{\nu}$  has been carried out in detail and discussed in section IV. Therefore, in the current study, we consider the parameters shown in Table X and Table XI for which the asymmetry is one, i.e.,  $H^- \rightarrow \tau_L^- \psi$ .

The polarisation of the  $\tau$  lepton is included in this analysis through TAUOLA [39]. We consider the hadronic one-prong decays of the  $\tau$  lepton — see the relations (8). For the signal in the MSSM, right-handed  $\tau_R^-$ 's come from the charged Higgs decay,  $H^- \rightarrow \tau_R^- \bar{\nu}$ , while in the backgrounds, left-handed  $\tau_L^-$ 's come from the decay of the  $W^- (\rightarrow \tau_L^- \bar{\nu})$ . In the MSSM, the requirement (9) would retain only the  $\pi$  and half of the longitudinal  $\rho$  and  $a_1$  contributions while eliminating the transverse components along with the other half of the longitudinal contributions. In addition, this requirement would suppress much of the backgrounds. In the framework of large extra dimensions, we are interested in  $H^- \rightarrow \tau_L^- \psi$  where, as shown in Fig. 6, the polarisation of the  $\tau$  lepton would be identical to the background case but opposite to the MSSM case. Therefore, the requirement (9) would not help in suppressing the backgrounds. Nevertheless, there are still some differences in the kinematics which can help reduce the background level, and the selection criteria are similar to the case presented in section IV, except here, we search for one-prong hadronic  $\tau$  decays (see [26] for further details):

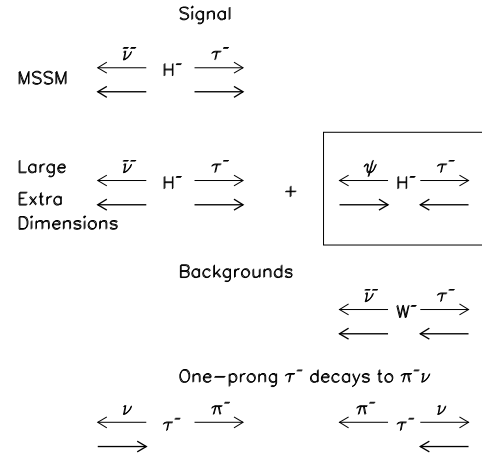


FIG. 6: Polarisation of the decay  $\tau$  from  $H^\pm$  in the MSSM and in models with a singlet neutrino in large extra dimensions. In the latter case, both left and right-handed  $\tau$ 's can be produced with some polarisation asymmetry. In the backgrounds, the  $\tau$  comes from the decay of the  $W^\pm$ . The signal to be studied is in the box — the polarisation of the decay  $\tau$  in this signal is the same as in the background. Thus,  $\tau$  polarisation effects would not help in suppressing the backgrounds but they may help distinguish between the 2HDM and other models.

1. The missing transverse momentum and the momentum of the  $\tau$  jet are increasingly harder as the charged Higgs mass increases.
2. The difference in the azimuthal opening angle between the  $\tau$  jet and the missing transverse momentum explained in section IV.
3. The difference in the transverse mass — Equation (11) — between the signal  $H^- \rightarrow \tau_L^- \psi$  and the background  $W^- \rightarrow \tau_L^- \bar{\nu}$ .

The reconstruction of the transverse mass (see Fig. 7)

TABLE XI: The expected rates ( $\sigma \times \text{BR}$ ), for the signal  $gb \rightarrow tH^\pm$  with  $H^\pm \rightarrow \tau_R^\pm \bar{\nu} + \tau_L^\pm \psi$  and  $t \rightarrow jjb$ , and for the backgrounds:  $Wt$  and  $t\bar{t}$  with  $W^- \rightarrow \tau_L^- \bar{\nu}$  and  $W^+ \rightarrow jj$ . We assume an inclusive  $t\bar{t}$  production cross section of 590 pb. Other cross sections are taken from PYTHIA 6.1. See Table X for the parameters used for Signal-1, Signal-2 and Signal-3. In the last columns, we compare the  $H^\pm \rightarrow \tau^\pm \nu_\tau$  branching ratios in this model to the corresponding MSSM branching ratios.

Process	$\sigma \times \text{BR}$ (pb)	$\text{BR}(H^\pm \rightarrow \tau\nu + \tau\psi)$	MSSM: $\text{BR}(H^\pm \rightarrow \tau^\pm \nu_\tau)$
Signal-1	1.56	0.73	0.37
Signal-2	0.15	1.0	0.15
Signal-3	0.04	1.0	0.01
$t\bar{t}$	84.11		
$gb \rightarrow Wt$ ( $p_T > 30$ GeV)	47.56		

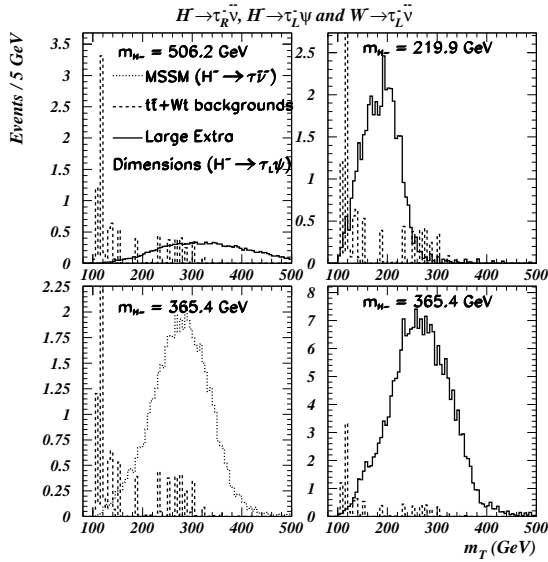


FIG. 7: The reconstructions of the transverse mass for the signal in the MSSM, the signal in models with a singlet neutrino in large extra dimensions and for the backgrounds, for an integrated luminosity of  $100 \text{ fb}^{-1}$ . In general, an MSSM charged Higgs can be discovered at the LHC depending on  $m_A$  and  $\tan\beta$ . In the models with a singlet neutrino in large extra dimensions, the signal can also be discovered at the LHC depending on the parameters  $M_*$ ,  $\delta$ ,  $m_D$ ,  $m_A$  and  $\tan\beta$ . The observation of the signal in the transverse mass distribution would not be sufficient to identify the model: the  $\tau$  polarisation effects must be explored further.

is not enough to distinguish between the MSSM and the singlet neutrinos in large extra dimensions. The differences in these two scenarios are best seen in the distribution of  $p^\pi/E^{\tau-jet}$ , the fraction of the energy carried by the charged track which is shown in Fig. 8.

The mass of the neutrino  $\psi$  would be different on an event by event basis. Consequently, the efficiencies of the kinematic cuts would be somewhat different. However, the main results of the current analysis derive from the differences in the polarisations of the  $\tau$  lepton and in the

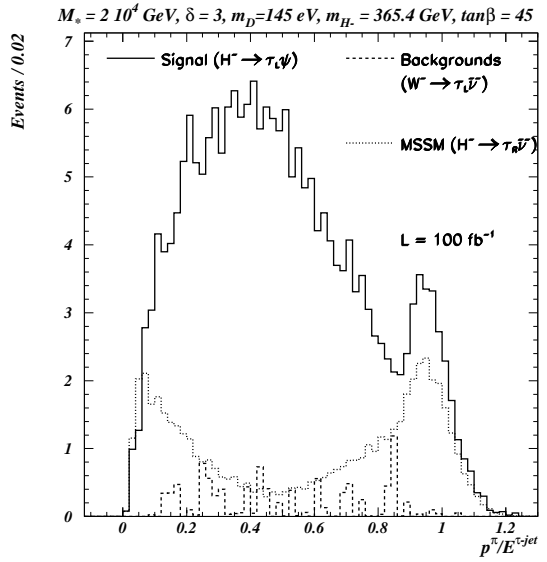


FIG. 8: The distribution of the ratio of the charged pion track momentum in one prong  $\tau$  decay to the  $\tau$ -jet energy for  $m_A = 350$  GeV,  $\tan\beta = 45$ ,  $M_* = 20$  TeV,  $\delta = 3$  and  $m_\nu = 0.05$  eV. In the 2HDM-II, this ratio would peak near 0 and 1 as shown while in other models, the actual distribution of this ratio would depend on the polarisation asymmetry since both left and right-handed  $\tau$ 's would contribute. In the case shown, the asymmetry is  $\sim 1$  and the ratio peaks near the centre of the distribution.

transverse mass bounds, and would not be significantly affected by the neutrino mass effect.

Although the observation of a signal in the transverse mass distribution can be used to claim discovery of the charged Higgs, it is insufficient to pin down the scenario that is realized. Additionally, by reconstructing the fraction of the energy carried by the charged track in the one-prong  $\tau$  decay, it is possible to claim whether the scenario is the ordinary 2HDM or not. The further measurement of the polarisation asymmetry might provide a distinctive evidence for models with singlet neutrinos in large extra dimensions.

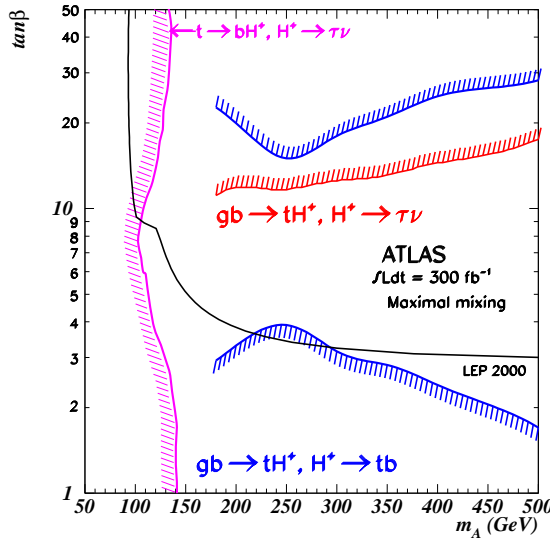


FIG. 9: The ATLAS 5- $\sigma$  discovery contour of the charged Higgs. Below the top quark mass, the charged Higgs is produced from top decay and the  $\tau^\pm\nu_\tau$  channel provides coverage for most  $\tan\beta$  below  $\sim 160$  GeV. Above the top quark mass, the  $tb$  channel covers the low and the high  $\tan\beta$  regions while the  $\tau^\pm\nu_\tau$  channel extends the discovery reach to high Higgs mass and to lower  $\tan\beta$  in the high  $\tan\beta$  region.

### VIII. $H^\pm$ DISCOVERY POTENTIAL

In the  $H^\pm \rightarrow tb$  channel, upwards of 5- $\sigma$  discovery can be achieved above the top quark mass in the low and high  $\tan\beta$  regions up to  $\sim 400$  GeV as discussed above [22].  $H^\pm \rightarrow \tau^\pm\nu_\tau$  extends the discovery reach to high Higgs masses and to lower  $\tan\beta$  values in the high  $\tan\beta$  region as seen in Fig. 9. However, in the low  $\tan\beta$  region, the  $\tau^\pm\nu_\tau$  channel offers no sensitivity for the charged Higgs discovery as the  $H^\pm \rightarrow \tau^\pm\nu_\tau$  branching vanishes [23]. Below the top quark mass, the charged Higgs is produced in top decays,  $t \rightarrow bH^\pm$ . In this mass range, the decay channel  $H^\pm \rightarrow \tau^\pm\nu_\tau$  has been studied for ATLAS and the signal appears as an excess of  $\tau$  leptons [55]: the entire range of  $\tan\beta$  values should be covered for  $m_{H^\pm} < m_t$  as shown in Fig. 9. The degradation of the sensitivity in the intermediate  $\tan\beta$  region is due to suppressed charged Higgs couplings to SM fermions as explained in section IX C.

Charged Higgs searches might be used to probe the decoupling regime of MSSM — hence distinguishing between SM and MSSM — particularly via the  $H^\pm \rightarrow \tau^\pm\nu_\tau$  channel. In fact, the extent of the parameter space that can be covered using this signature is comparable to the reach of the  $A/H \rightarrow \tau\tau$  channel in the neutral Higgs sector, at least at large  $\tan\beta$  [23, 32, 44, 56]. Furthermore, additional improvements may still be possible in the  $H^\pm \rightarrow \tau^\pm\nu_\tau$  channel such as the possibility of exploiting

the kinematics of the spectator  $b$ -jet in  $gg \rightarrow tbH^\pm$  and the recent calculation of a rather large k-factor for  $gb \rightarrow tH^\pm$  [57].

## IX. OUTLOOK

In this section, we discuss additional work planned or currently being carried out in the charged Higgs sector to study the region below the top quark mass, the prospects for  $m_{H^\pm}$  determination in this region, and also to cover the remaining areas of the discovery contour of Fig. 9.

### A. Below the top quark mass

The  $H^\pm \rightarrow \tau^\pm\nu_\tau$  channel is currently being investigated further, taking into account the  $\tau$  polarisation effects. A direct measurement of the charged Higgs mass in this region is not possible because of the presence of various neutrinos in the final state. The possibility of measuring the charged Higgs mass from the  $\tau - b$  system in the final state is being studied.

### B. Threshold Region

For  $m_{H^\pm}$  just below or around the top quark mass, the relevant channels are  $H^\pm \rightarrow t^*b$  and  $H^\pm \rightarrow \tau^\pm\nu_\tau$ . The correct description of the charged Higgs production and decay mechanisms in this region of parameter space requires the use the production process  $gg \rightarrow tbH^\pm$ , shown in Fig. 1 which includes  $gg \rightarrow t\bar{t}$  with  $t \rightarrow bH^\pm$ , the Higgs-strahlung mechanism and the relative interferences [58]: the narrow width approximation used by Monte Carlo programs such as PYTHIA [27], HERWIG [59] and ISAJET [60], accounts for the charged Higgs production and decay through the factorisation approach, i.e.,  $gg, q\bar{q} \rightarrow t\bar{t}$  times  $t \rightarrow bH^\pm$ . However, this description does not account properly for the charged Higgs boson phenomenology when its mass approaches or exceeds that of the top quark as shown in Fig. 10 [58, 61]. For the LHC, the situation is further complicated by the potential problem of double counting when adding the  $2 \rightarrow 3$  and the  $2 \rightarrow 2$  production mechanisms of Fig. 1. The 5- $\sigma$  discovery contour of Fig. 9 shows a gap in the  $m_A$  axis around  $m_A = 160$  GeV corresponding to the threshold region where studies have just commenced using the  $gg \rightarrow tbH^\pm$  instead of the factorisation approach.

### C. Intermediate $\tan\beta$ Region

In the studies discussed thus far, a heavy SUSY spectrum has been assumed; thus charged Higgs decays into supersymmetric particles are kinematically forbidden. The lack of sensitivity in the intermediate  $\tan\beta$  region

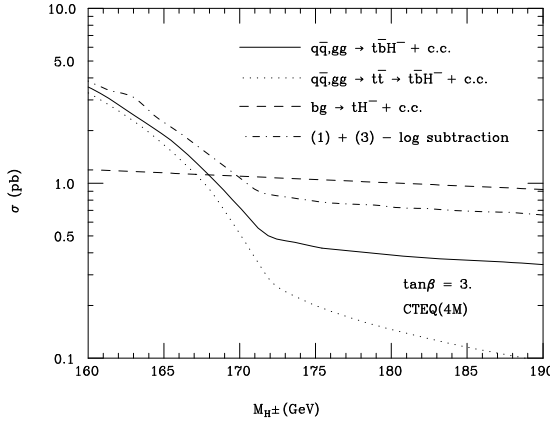


FIG. 10: Cross section for  $gg, q\bar{q} \rightarrow t\bar{b}H^\pm$ ;  $gg, q\bar{q} \rightarrow t\bar{t} \rightarrow t\bar{b}H^\pm$  with finite top quark width;  $bg \rightarrow tH^\pm$  and the combination of the first and the last, at the LHC with  $\sqrt{s} = 14$  TeV, as a function of  $m_{H^\pm}$  for a representative value of  $\tan\beta$ .

( $\tan\beta \sim 3\text{-}10$ ) is due to the fact that the charged Higgs coupling to SM fermions is proportional to:

$$H^+(m_t \cot\beta \bar{t}b_L + m_b \tan\beta \bar{t}b_R), \quad (29)$$

the square of which goes through a minimum at  $\tan\beta = \sqrt{m_t/m_b}$ . The study of charged Higgs decays into SUSY particles might help cover this region. Indeed, for a heavy charged Higgs boson, the decays into the lightest charginos and neutralinos — sleptons and squarks also — would be possible and even become dominant, thereby reducing the branching into the SM decays  $H^\pm \rightarrow tb$  and  $H^\pm \rightarrow \tau^\pm \nu_\tau$  [62]. It was shown in [63] that  $H^\pm \rightarrow \tilde{\chi}_1^\pm \tilde{\chi}_{2,3}^0$  could probe regions of the MSSM parameter space where the  $H^\pm$  decays into SM particles yield no sensitivity — see Fig. 9. In addition to the direct  $H^\pm$  production via the  $2 \rightarrow 3$  and the  $2 \rightarrow 2$  processes of Fig. 1, the  $H^\pm$  production rate in SUSY particle cascade decays can be significant and sensitive to the intermediate  $\tan\beta$  values [64]. Further studies of these exotic charged Higgs decays are in progress [65].

#### D. High Mass Region

The discovery reach could be extended to higher Higgs masses by studying the process  $gg \rightarrow tbH^\pm$  with  $H^\pm \rightarrow tb$  and tagging all the four  $b$ -jets in the spectrum [40] and exploiting the differences between the signal and the  $gg \rightarrow t\bar{t}b\bar{b}$  background in the kinematics of  $b$ -quark jets: in the background, the  $b$ -quark pair produced together with  $t\bar{t}$  are rather soft, collinear with low invariant mass. On the contrary, in the signal, at least one of the associated  $b$ -jets is expected to be energetic for  $m_{H^\pm}$  much larger than  $m_t$  [40]. However, tagging four  $b$ -jets may cause a significant reduction in the signal rate as the

additional  $b$ -quark in  $gg \rightarrow tbH^\pm$  has a low transverse momentum and may escape detection. Realistic studies of this channel including detector effects are in progress.

## X. CONCLUSIONS

In the simplest extension of the SM Higgs sector, five Higgs bosons are predicted, three neutral and a charged pair. The charged Higgs boson does not have a SM counterpart, thus its discovery would constitute an irrefutable evidence of physics beyond the Standard Model.

In this paper, we have investigated the feasibility of the charged Higgs detection at the LHC with the ATLAS detector. Below the top quark mass,  $H^\pm$  could be produced in the decay of the top quark,  $t \rightarrow bH^\pm$ , and the decay  $H^\pm \rightarrow \tau^\pm \nu_\tau$  was previously studied for ATLAS. The signal appears as an excess of  $\tau$  leptons and almost the entire range of  $\tan\beta$  is covered. In the LEP allowed regions of MSSM parameter space, the  $H^\pm \rightarrow W^\pm h^0$  channel presents no significant discovery potential for the charged Higgs. In NMSSM, LEP constraints are no longer valid and the signal viability is extended to a bigger area of parameter space.

In the  $H^\pm \rightarrow tb$  channel, upwards of 5- $\sigma$  discovery can be achieved above the top quark mass in the low and high  $\tan\beta$  regions up to  $\sim 400$  GeV. The  $H^\pm \rightarrow \tau^\pm \nu_\tau$  channel extends the discovery reach to higher Higgs masses and to lower  $\tan\beta$  values but the sensitivity is limited to the high  $\tan\beta$  region. In models with singlet neutrinos in large extra dimensions, the process  $H^\pm \rightarrow \tau_L^- \psi + c.c.$  — which is completely suppressed in the 2HDM — can have a significant branching ratio, and its detection together with the measurement of the  $\tau$  polarisation asymmetry would provide a distinctive evidence for these models.

The charged Higgs mass can be determined in  $H^\pm \rightarrow tb$  and  $H^\pm \rightarrow \tau^\pm \nu_\tau$  where the precisions range from 0.5% at  $\sim 200$  GeV to 1.8% at  $\sim 500$  GeV for an integrated luminosity of  $300 \text{ fb}^{-1}$ . In either channel, the main uncertainties come from statistical errors in the invariant mass ( $H^\pm \rightarrow tb$ ) or the transverse mass ( $H^\pm \rightarrow \tau^\pm \nu_\tau$ ) distributions. By measuring the rate of  $H^\pm \rightarrow \tau^\pm \nu_\tau$ ,  $\tan\beta$  can be determined with precisions ranging from 7.4% at  $\tan\beta = 20$  to 5.4% at  $\tan\beta = 50$  for an integrated luminosity of  $300 \text{ fb}^{-1}$  and assuming a 10% uncertainty on the luminosity.

Further charged Higgs studies are planned or are currently being carried out in order to cover the remaining regions of the parameter space. These include: firstly, the threshold region where the  $2 \rightarrow 3$  process is used to correctly account for the  $H^\pm$  production and decay phenomenology; secondly, the intermediate  $\tan\beta$  region which is sensitive to charged Higgs decays to SUSY particles; and finally, the high mass region which could be probed with  $gg \rightarrow tbH^\pm$  and  $H^\pm \rightarrow tb$  by tagging all the four  $b$ -jets in the spectrum. In addition, the region below the top quark mass is being investigated using  $H^\pm \rightarrow \tau^\pm \nu_\tau$  taking into account the  $\tau$ -polarisation ef-

fects, and the prospects for  $m_{H^\pm}$  determination in this region is also being studied.

### Acknowledgments

We express gratitude to E. Richter-Was, K. Jacobs and the ATLAS Higgs working group for fruitful discussions and constructive criticisms. This work was mainly performed within the ATLAS collaboration and we thank the collaboration members for helpful discussions. Parts

of this work were carried out at the Les Houches Workshop: “Physics at TeV Colliders” 1999 and 2001. We thank the organisers for the invitation and for their effort. K. A. Assamagan thanks K. Agashe for helpful correspondence, and S. Moretti and R. Kinnunen for useful discussions. K. A. Assamagan’s contribution was partially supported by grants from the US National Science Foundation (grant numbers 9722827 and PHY-0072686) at Hampton University prior to his appointment at Brookhaven National Laboratory.

---

- [1] J.F. Gunion, H.E. Haber, G.L. Kane, S. Dawson, The Higgs Hunter’s Guide (Addison-Wesley, Reading, MA 1990), Erratum: arXiv:hep-ph/9302272; H. P. Nilles, Phys. Rept. **110**, 1 (1984); H. E. Haber and G. L. Kane, Phys. Rept. **117**, 75 (1985).
- [2] S. Heinemeyer, W. Hollik and G. Weiglein, Eur. Phys. J. C **9**, 343 (1999) [arXiv:hep-ph/9812472].
- [3] The ALEPH, DELPHI, L3 and OPAL Collaborations and the LEP Higgs Working Group, CERN-EP/2001-055, arXiv:hep-ex/0107030.
- [4] The LEP Electroweak Working Group, A Combination of Preliminary Electroweak Measurements and Constraints in the Standard Model, CERN-EP/2001- in preparation, presented by D. Charlton, EPS HEP 2001, Budapest, Hungary, July 12-18, 2001.
- [5] L. Moneta, talk given at the ‘36th Rencontres de Moriond on QCD and Hadronic Interactions’, Les Arcs, France, 17-24 March 2001, arXiv:hep-ex/0106050.
- [6] G. Abbiendi, OPAL Collaboration, Eur. Phys. J. C **18**, 425, (2001) [arXiv:hep-ex/0007040].
- [7] A. Brignole, J. Ellis, G. Ridolfi, F. Zwirner, Phys. Lett. B **271**, 123 (1991); A. Brignole, Phys. Lett. B **277**, 313 (1992); M. A. Diaz, H. E. Haber, Phys Rev. D **45**, 4246 (1992).
- [8] ALEPH, DELPHI, L3 and OPAL Collaborations, CERN-EP/2000-055; ALEPH Collaboration, CERN-EP/2000-086, Phys. Lett. B487 (2000) 253; DELPHI Collaboration, CERN-EP/2001-062, M. Ellert et al., Nucl. Phys. B – Proceeding supplements 98 (2001), 336; L3 Collaboration, CERN-EP/2000-118, Phys. Lett. B496 (2000) 34; OPAL Collaboration, CERN-EP/98-173.
- [9] P. Gutierrez, FERMILAB-Conf-00-294-E; V. M. Abazov *et al.* [DØ Collaboration], arXiv:hep-ex/0102039.
- [10] M. S. Alam *et al.* [CLEO Collaboration], Phys. Rev. Lett. **74**, 2885 (1995); R. Briere, in Proceedings of ICHEP98, Vancouver Canada, 1998, CLEO-CONF-98-17; *ibid.* and in talk by J. Alexander; R. Barate *et al.* [ALEPH Collaboration], Phys. Lett. B **429**, 169 (1998).
- [11] F. M. Borzumati and C. Greub, Phys. Rev. D **58**, 074004 (1998) [arXiv:hep-ph/9802391]; Phys. Rev. D **59**, 057501 (1999) [arXiv:hep-ph/9809438].
- [12] J. A. Coarasa, J. Guasch, J. Sola and W. Hollik, Phys. Lett. B **442**, 326 (1998) [arXiv:hep-ph/9808278].
- [13] J. F. Gunion, H. E. Haber, F. E. Paige, W. K. Tung and S. S. Willenbrock, Nucl. Phys. B **294**, 621 (1987); J. L. Diaz-Cruz and O. A. Sampayo, Phys. Rev. D **50**, 6820 (1994).
- [14] A. Krause, T. Plehn, M. Spira and P. M. Zerwas, Nucl. Phys. B **519**, 85 (1998) [arXiv:hep-ph/9707430]; Y. Jiang, W. g. Ma, L. Han, M. Han and Z. h. Yu, J. Phys. G **24**, 83 (1998) [arXiv:hep-ph/9708421]; A. A. Barrientos Bendezu and B. A. Kniehl, Nucl. Phys. B **568**, 305 (2000) [arXiv:hep-ph/9908385]; O. Brein and W. Hollik, Eur. Phys. J. C **13**, 175 (2000) [arXiv:hep-ph/9908529].
- [15] D. A. Dicus, J. L. Hewett, C. Kao and T. G. Rizzo, Phys. Rev. D **40**, 787 (1989); A. A. Barrientos Bendezu and B. A. Kniehl, Phys. Rev. D **59**, 015009 (1999) [arXiv:hep-ph/9807480]; Phys. Rev. D **61**, 097701 (2000) [arXiv:hep-ph/9909502]; Phys. Rev. D **63**, 015009 (2001) [arXiv:hep-ph/0007336]; O. Brein, W. Hollik and S. Kanemura, Phys. Rev. D **63**, 095001 (2001) [arXiv:hep-ph/0008308].
- [16] S. Moretti and K. Odagiri, Phys. Rev. D **59**, 055008, (1999).
- [17] F. Borzumati, J. L. Kneur and N. Polonsky, Phys. Rev. D **60**, 115011 (1999) [arXiv:hep-ph/9905443].
- [18] S. Moretti and D. P. Roy, Phys. Lett. B **470**, 209 (1999) [arXiv:hep-ph/9909435].
- [19] A. Djouadi *et al.*, “The Higgs working group: Summary report,” Proceedings of the Workshop ‘Physics at TeV Colliders’, Les Houches, France, 8-18 June 1999, arXiv:hep-ph/0002258; D. Denegri *et al.*, arXiv:hep-ph/0112045.
- [20] A. Belyaev, D. Garcia, J. Guasch and J. Sola, Phys. Rev. D **65**, 031701 (2002) [arXiv:hep-ph/0105053].
- [21] A. Djouadi, J. Kalinowski and M. Spira, Comput. Phys. Commun. **108**, 56 (1998) [arXiv:hep-ph/9704448].
- [22] K. A. Assamagan, Acta Phys. Polon. B **31**, 863 (2000); ATLAS Internal Note ATL-PHYS-99-013.
- [23] K.A. Assamagan and Y. Coadou, Acta Phys. Polon. B **33**, 707 (2002); ATLAS Internal Note ATL-PHYS-2000-031 (2000).
- [24] K.A. Assamagan, Acta Phys. Polon. B **31**, 881 (2000); ATLAS Internal Note ATL-PHYS-99-025.
- [25] K.A. Assamagan and Y. Coadou, ATLAS Internal Note ATL-PHYS-2001-017 (2001).
- [26] K. A. Assamagan and A. Deandrea, ATLAS Internal Note ATL-PHYS-2001-019, Phys. Rev. D in press, arXiv:hep-ph/0111256.
- [27] T. Sjostrand, Comput. Phys. Commun. **82**, 74 (1994); T. Sjostrand, P. Eden, C. Friberg, L. Lonnblad, G. Miu, S. Mrenna and E. Norrbin, Comput. Phys. Commun. **135**, 238 (2001) [arXiv:hep-ph/0010017]; T. Sjostrand, L. Lonnblad and S. Mrenna, arXiv:hep-ph/0108264.

[28] E. Richter-Wąs, D. Froidevaux and L. Poggioli, ATLAS Internal Note, ATL-PHYS-98-131, (1998).

[29] H. L. Lai *et al.*, Phys. Rev. D **55**, 1280 (1997) [arXiv:hep-ph/9606399].

[30] S. Heinemeyer, W. Hollik and G. Weiglein, arXiv:hep-ph/0002213.

[31] ATLAS Collaboration, Technical Proposal for a General Purpose pp Experiment at the Large Hadron Collider at CERN, CERN/LHCC/94-43, LHCC/P2, 15 December 1994.

[32] ATLAS Collaboration, 'ATLAS Detector and Physics Performance Technical Design Report', CERN/LHCC/99-15, 25 May (1999) 285.

[33] M. Bosman, Talk given at the IX International Conference on Calorimetry in Particle Physics, October 9-14, 2000, Annecy, France, ATL-CONF-2002-001 (2002)

[34] V. D. Barger, R. J. Phillips and D. P. Roy, Phys. Lett. B **324**, 236 (1994) [arXiv:hep-ph/9311372].

[35] K. Odagiri, RAL-TR-1999-012; hep-ph/9901432.

[36] D. P. Roy, Phys. Lett. B **459**, 607 (1999) [arXiv:hep-ph/9905542].

[37] B. K. Bullock, K. Hagiwara and A. D. Martin, Nucl. Phys. B **395**, 499 (1993).

[38] S. Raychaudhuri and D. P. Roy, Phys. Rev. D **52**, 1556 (1995) [arXiv:hep-ph/9503251]; Phys. Rev. D **53**, 4902 (1996) [arXiv:hep-ph/9507388].

[39] S. Jadach, Z. Wąs, R. Decker and J. H. Kühn, Comput. Phys. Commun. **76**, 361 (1993); M. Jezabek, Z. Wąs, S. Jadach and J. H. Kühn, Comput. Phys. Commun. **70**, 69 (1992); S. Jadach, J. H. Kühn and Z. Wąs, Comput. Phys. Commun. **64**, 275 (1990).

[40] D. J. Miller, S. Moretti, D. P. Roy and W. J. Stirling, Phys. Rev. D **61**, 055011 (2000) [arXiv:hep-ph/9906230].

[41] S. Moretti and W. J. Stirling, Phys. Lett. B **347**, 291 (1995) [Erratum-ibid. B **366**, 451 (1996)] [arXiv:hep-ph/9412209]; A. Djouadi, J. Kalinowski and P.M. Zerwas, Z. Phys. C70 (1996) 435; E. Ma, D.P. Roy and J. Wudka, Phys. Rev. Lett. 80 (1998) 1162.

[42] M. Drees, M. Guchait and D. P. Roy, Phys. Lett. B **471**, 39 (1999) [arXiv:hep-ph/9909266] and the references therein.

[43] S. Moretti, Phys. Lett. B **481**, 49, (2000); [ArXiv:hep-ph/0003178].

[44] R. Kinnunen, "The  $H^\pm \rightarrow \tau^\pm \nu_\tau$  mode in CMS" and "Signatures of Heavy Charged Higgs Bosons at the LHC", Les Houches Workshop (1999), hep-ph/0002258; D. Denegri *et al.*, CMS Internal Note CMS-NOTE-2001-032, hep-ph/0112045.

[45] M. Hohlfeld, ATLAS Internal Note ATL-PHYS-2001-004 (2001).

[46] J. F. Gunion, L. Poggioli, R. Van Kooten, C. Kao and P. Rowson, arXiv:hep-ph/9703330.

[47] T. Kaluza, Sitzungsber. Preuss. Akad. Wiss. Berlin (Math. Phys. ) **K1**, 966 (1921); for a translation of the original paper see T. Muta, HUPD-8401 *in O'Raifeartaigh, L.: The dawning of gauge theory\** 53-58; O. Klein, Z. Phys. **37**, 895 (1926) [Surveys High Energ. Phys. **5**, 241 (1926)].

[48] N. Arkani-Hamed, S. Dimopoulos and G. R. Dvali, Phys. Lett. B **429**, 263 (1998) [arXiv:hep-ph/9803315]; Phys. Rev. D **59**, 086004 (1999) [arXiv:hep-ph/9807344]; I. Antoniadis, N. Arkani-Hamed, S. Dimopoulos and G. R. Dvali, Phys. Lett. B **436**, 257 (1998) [arXiv:hep-ph/9804398]; G. F. Giudice, R. Rattazzi and J. D. Wells, Nucl. Phys. B **544**, 3 (1999) [arXiv:hep-ph/9811291]; E. A. Mirabelli, M. Perelstein and M. E. Peskin, Phys. Rev. Lett. **82**, 2236 (1999) [arXiv:hep-ph/9811337]; T. Han, J. D. Lykken and R. J. Zhang, Phys. Rev. D **59**, 105006 (1999) [arXiv:hep-ph/9811350].

[49] N. Arkani-Hamed, S. Dimopoulos, G. R. Dvali and J. March-Russell, arXiv:hep-ph/9811448. K. R. Dienes, E. Dudas and T. Gherghetta, Nucl. Phys. B **557**, 25 (1999) [arXiv:hep-ph/9811428].

[50] K. Akama, Lect. Notes Phys. **176**, 267 (1982) [arXiv:hep-th/0001113]; V. A. Rubakov and M. E. Shaposhnikov, Phys. Lett. B **125** (1983) 136; for a review see V. A. Rubakov, "Large and infinite extra dimensions: An Introduction," arXiv:hep-ph/0104152.

[51] J. Polchinski, arXiv:hep-th/9611050. C. P. Bachas, arXiv:hep-th/9806199.

[52] S. P. Martin and J. D. Wells, Phys. Rev. D **60**, 035006 (1999) [arXiv:hep-ph/9903259].

[53] Y. Fukuda *et al.* [SuperKamiokande Collaboration], Phys. Rev. Lett. **82**, 2644 (1999) [arXiv:hep-ex/9812014]; **85**, 3999 (2000) [arXiv:hep-ex/0009001]; **86**, 5656 (2001) [arXiv:hep-ex/0103033]; A. Ioannisian and A. Pilaftsis, Phys. Rev. D **62**, 066001 (2000) [arXiv:hep-ph/9907522]. R. N. Mohapatra and A. Perez-Lorenzana, Nucl. Phys. B **576**, 466 (2000) [arXiv:hep-ph/9910474]; A. S. Dighe and A. S. Joshipura, Phys. Rev. D **64**, 073012 (2001) [arXiv:hep-ph/0105288]; A. De Gouvea, G. F. Giudice, A. Strumia and K. Tobe, arXiv:hep-ph/0107156.

[54] K. Agashe, N. G. Deshpande and G. H. Wu, Phys. Lett. B **489**, 367 (2000) [arXiv:hep-ph/0006122].

[55] D. Cavalli *et al.*, ATLAS Internal Note ATL-PHYS-94-053 (1994).

[56] D. Cavalli and S. Resconi, ATLAS Internal Note ATL-PHYS-2000-005 (2000).

[57] S.-H. Zhu, arXiv:hep-ph/0112109.

[58] M. Guchait and S. Moretti, JHEP **0201**, 001 (2002) [arXiv:hep-ph/0110020].

[59] G. Marchesini, B. R. Webber, G. Abbiendi, I. G. Knowles, M. H. Seymour and L. Stanco, Comput. Phys. Commun. **67**, 465 (1992). G. Corcella *et al.*, arXiv:hep-ph/9912396. G. Corcella *et al.*, arXiv:hep-ph/0107071, arXiv:hep-ph/0201201.

[60] H. Baer, F. E. Paige, S. D. Protopopescu and X. Tata, arXiv:hep-ph/0001086.

[61] S. Moretti, private communication.

[62] F. Borzumati and A. Djouadi, hep-ph/9806301; P. M. Zerwas *et al.*, ECFA-DESY Workshop, hep-ph/9605437.

[63] M. Bisset, M. Guchait and S. Moretti, Eur. Phys. J. C **19**, 143 (2001) [arXiv:hep-ph/0010253].

[64] A. Datta, A. Djouadi, M. Guchait and Y. Mambrini, Phys. Rev. D **65**, 015007 (2002) [arXiv:hep-ph/0107271].

[65] M. Bisset, F. Moortgat and S. Moretti, in preparation.